Texture, nanotexture, and structure of carbon nanotube-supported carbon cones

Germercy Paredes, Rongrong Wang, Pascal Puech, Grégory Seine, Jean-Marc Leyssale, Raul Arenal, Aurélien Masseboeuf, Fabrice Piazza, Marc Monthioux

Texture, nanotexture, and structure of carbon nanotube-supported carbon cones

Germercy Paredes[1,2,*], Rongrong Wang[1,3], Pascal Puech[1], Grégory Seine[1], Jean-Marc Leyssale[4], Raul Arenal[3,5,6], Aurélien Masseboeuf[1], Fabrice Piazza[2], Marc Monthioux[1,*]

[1]*Centre d'Elaboration des Matériaux et d'Etudes Structurales (CEMES), UPR8011 CNRS, Université Toulouse 3, 31055 Toulouse, France.*

[2]*Laboratorio de Nanociencia, Pontificia Universidad Católica Madre y Maestra, Santiago de Los Caballeros 51000, Dominican Republic.*

[3]*Laboratorio de Microscopias Avanzadas (LMA), Universidad de Zaragoza, 50018 Zaragoza, Spain.*

[4]*Univ. Bordeaux, CNRS, Bordeaux INP, Institut des Sciences Moléculaires (ISM), UMR 5255, F-33400 Talence, France.*

[5]*Fundación ARAID, 50018 Zaragoza, Spain.*

[6]*Instituto de Nanociencia y Materiales de Aragon (INMA), CSIC-U. Zaragoza, 50009 Zaragoza, Spain.*

ABSTRACT: Graphene-based carbon micro-/nano-cones were prepared by depositing pyrolytic carbon onto individual carbon nanotubes as supports using a specific chemical vapor deposition process. They were investigated by means of high-resolution scanning electron microscopy, low-voltage aberration-corrected transmission electron microscopy, Raman spectroscopy, and molecular dynamics modelling. While the graphenes were confirmed to be perfect, the cone texture was determined to be preferably scroll-like, with the scroll turns being parallel to the cone axis. Correspondingly, many of the concentrically-displayed graphenes (actually scroll turns) exhibit the same helicity vector. When radii of curvature are large enough, this could allow for coherent stacking to locally take place in spite of the lattice shift induced by the curvature. A particular care was taken on investigating the cone apices, in which a specific type of graphene termination was observed, here designated as "zip" defect. Calculations determined a plausible stable structure that such a defect type may correspond to. This defect was found to generate the a very low Raman $I_D/I_{D'}$ band ratio (1.5), for which physical reasons are proposed. Combining our results and that of the literature allowed proposing an identification chart for a variety of defects able to affect the graphene lattice or edges.

* Corresponding authors.
E-mail addresses: gd.paredes@ce.pucmm.edu.do (G. Paredes); marc.monthioux@cemes.fr (M. Monthioux)

KEYWORDS: *nanocones, scroll texture, graphene defects, Raman spectroscopy, high resolution TEM, Molecular dynamics*

It is now of common knowledge that carbon atoms can build up an amazing variety of sp^2-C- or sp^3-C-based nano- to micro-scale morphologies, among them conical ones. Carbon conical morphologies are interesting as they can be useful for a variety of applications such as electron emission[1-5] and near-field microscopy probes[6,7] with an unbeatable superiority over other materials thanks to the properties of the resulting objects in terms of electrical and/or thermal conductivity, current density, and mechanical behavior, among others. An original way to grow carbon micro-to-nano-cones was proposed years ago, based on a time-of-flight chemical vapor deposition (ToF-CVD) process using multi-wall carbon nanotubes (CNTs) as individual supports for the formation of individual cones.[8,9]

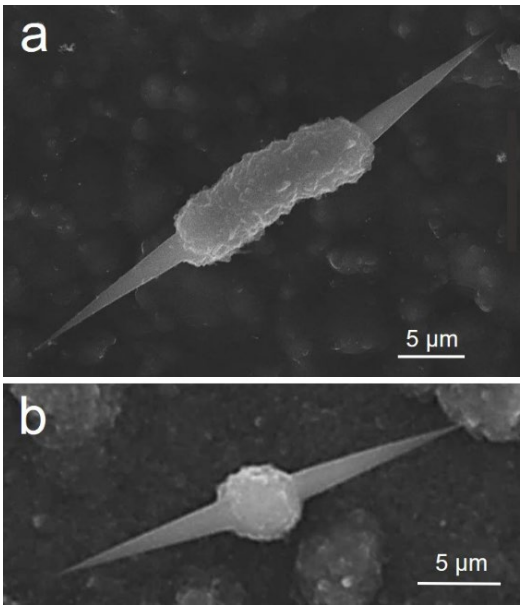

Figure 1. Typical examples of the carbon cone-bearing objects obtained from the ToF-CVD process.

Figure 1 provides examples of the current production of such carbon cones, showing a combination of opposed cones protruding from a graphenic micro-object with rough surface and more or less elongated, hence looking like either a fiber-segment (**Figure 1a**) or a bead (**Figure 1b**). Such complex morphologies are typical of the cones prepared by our ToF-CVD process. The microsized carbon part bearing the cones is very useful for subsequent applications, for allowing the objects to be individually located, handled, mounted, aligned, and fixed without damaging the cone, even under an optical microscope.[1,7] An amazing statement is that the smooth-cone parts and

the rough-surface bead or fiber-segment part both grow in the same time, necessarily originating from complex growth mechanisms, which were just elucidated.[10] Briefly, they involve the role of a transient liquid phase which forms in spite of the high furnace temperature (1400°C) and that of wetting phenomena which occur within the time range of microseconds,[10] as tentatively summarized in Figure 2.

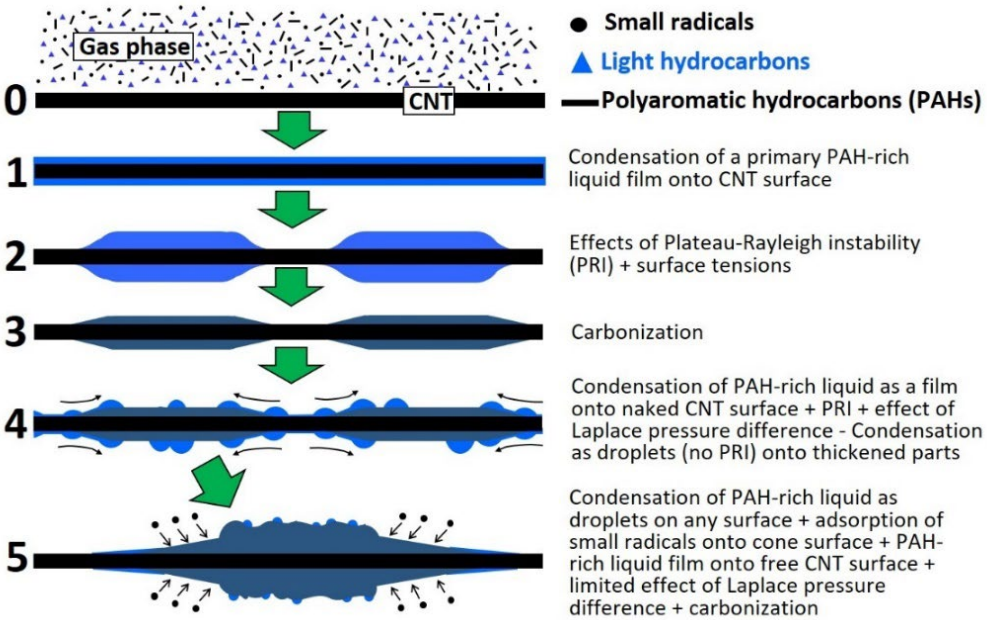

Figure 2. Sketch of the growth scenario for carbon objects as shown in **Figure 1a**, as stated in Paredes *et al.*.[10] Elements are not at scale, and the successive steps do not correspond to equal time-periods. **Step 0:** a previously-grown CNT and a gas phase with complex chemical composition (as a consequence of the ToF-CVD conditions) are in contact. **Step 1:** the gas phase, which contains polyaromatic hydrocarbons (PAHs), condenses as an organic liquid cylinder around the CNT. **Step 2:** The Plateau-Rayleigh instability (PRI) combined with the specific rheological behavior of the liquid break the liquid film and form nanosized, axisymmetric spindle-shape droplets periodically displayed along the CNT; surface tensions make the PAHs to align parallel to the CNT surface. **Step 3:** carbonization proceeds, forming concentric graphene cylinders and primary cones; graphene edges at the conical part surface make the first adsorption sites. **Step 4:** as a well-known mechanism in pyrolytic carbon deposition processes,[11] radicals require adsorption sites to be captured, hence the contribution of radicals to the growth is still very limited at that time; on the other hand, the PAH-containing liquid can keep depositing everywhere; when depositing on the thickened parts of the CNT, a liquid film cannot form anymore (diameter is too large), hence PAHs deposit under another form instead; but when depositing on the naked parts of the CNT, a liquid cylinder can still condense, but the contacts of the liquid film with the conical parts make that the droplets created by the PRI are subjected to a Laplace pressure difference; this makes the axisymmetric droplets to migrate towards the base of the cone parts, leaving the CNT surface naked; the migration stops once the droplets reach the cone part where the diameter is too large for the droplets to remain axisymmetric; therefore, the more the cones grow, the shorter the droplet migration is. **Step 5** (magnification of the related sketch is reduced with respect to that of the previous steps)**:** the carbonization proceeds while Step-4 events keep going; PAHs not subjected to the PRI do not align well, resulting in somewhat isotropically-displayed distorted graphenes, hence the rough surface of the fiber-like part; in droplets resulting from the PRI, PAHs are subjected to surface tensions and resulting graphenes align

well, hence the concentric display of graphenes, the presence of many graphene free-edges at the cone surface, and the smooth surface; from this step, the cones mostly grow from the radicals, while the fiber-part mostly grows from the PAHs. The figure is reprinted in part and completed with permission under a CC-BY-NC-ND license from Paredes *et al.* Unveiling the Existence and Role of a Liquid Phase in a High Temperature (1400 °C) Pyrolytic Carbon Deposition Process. *Carbon Trends* **2021**, *5,* 10017,[10] Copyright 2021 by the Authors.

Previous textural and structural studies demonstrated that the cones were entirely built with high-quality nanotexture graphenes, with the graphenes displayed and oriented concentrically around each individual primary CNT (**Figure 3**), from which a Russian-doll model of concentric graphene cylinders was assumed, with many of the graphenes exhibiting the same helicity.[12] The cone surface therefore exhibits graphene steps all along the cone while the number of concentric graphenes decreases from the base to the tip, hence generating the conical morphology.[12]

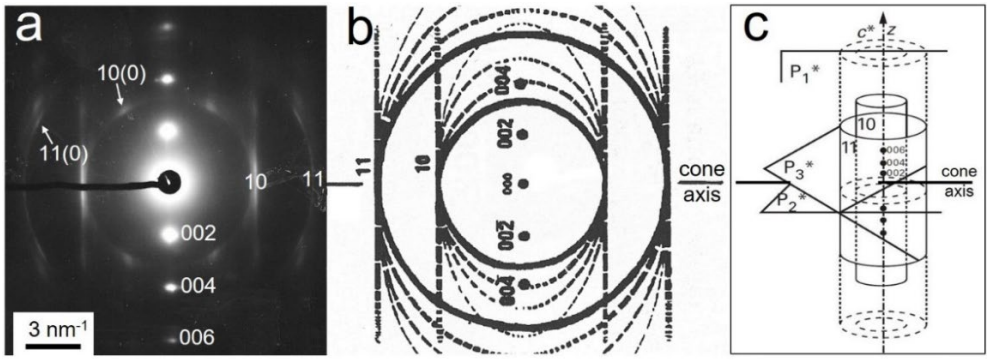

Figure 3. (a) Electron diffraction pattern (at 120 keV) of part of a cone seen longitudinally, with the cone axis in the image plane and perpendicular to the [*00l*] direction; the pattern shows a combination of faint rings, lines, and spots; reprinted with permission from Allouche *et al.* Chemical Vapor Deposition of Pyrolytic Carbon on Carbon Nanotubes. Part 2. Texture and Structure. *Carbon* **2005**, *43*, 1265-1278,[12] Copyright 2005 by Elsevier. **(b)** Sketch of part of a diffraction pattern such as in (a); reprinted with permission from Monthioux, M. Structure, Texture, and Thermal Behaviour of Polyaromatic Solids. In *Carbon Molecules and Materials*; Setton, R., Bernier, P., Lefrant, S., Eds.; Taylor & Francis, London (UK), **2002**; pp.127-177,[13] Copyright 2002 by Taylor & Francis. **(c)** Sketch of the reciprocal image of a graphene stack with the turbostratic structure to explain some of the specific features of the diffraction pattern sketched in (b); reprinted with permission from Oberlin *et al*. Techniques d'Etude des Structures et Textures (Microtextures) des Matériaux Carbonés. *J. Chim. Phys.* **1984**, *81*, 701-710,[14] Copyright 1984 by EDP Sciences. In (c), *hk* reciprocal elements appear as elongated cylinders because all the possible graphene rotational orientations are found in the stack, and each graphene is considered as a one-atom-thick crystal by the incoming electrons; the only reciprocal elements for which all the graphenes contribute altogether as in a single crystal are the *00l* ones, hence they are not elongated but spots because all the graphenes are parallel to the P_2* plane. Assuming that, in the cone, all the graphenes are concentrically displayed, the reciprocal image of it is obtained by rotating the reciprocal cylinders in (c) around the cone axis, and the diffraction patterns in (a) and (b) result from the intersection of the concentric cylinders by various planes in (c) such as P_1*, which generates the lines, P_2*, which generates the rings, and P_3* and all the planes in-between, which generate the ellipses. However, in addition to those features typical of the turbostratic structure, the

diffraction pattern in (a) shows *hk(0)* spots (two are arrowed) distributed according to the hexagonal symmetry, which indicate that at least part of the concentric graphenes exhibit the same helicity (here of zigzag type (*n,0*)).

However, an accurate study of the graphene configuration within the cones was missing, especially at the apices. This is what is addressed in this paper, by investigating how the cones behave when passing an electron flow through them, and studying textural and structural aspects by combining scanning electron microscopy (SEM), high resolution transmission electron microscopy (HRTEM), and Raman spectroscopy.

RESULTS AND DISCUSSION

Russian-doll *versus* scroll models. Figure 4 provides a series of SEM images of several cones. Cones with a periodically undulated surface such as illustrated in **Figures 4a-b** were in minor occurrence, but they attracted attention because the positions of the bumps on both sides of the cone silhouettes suggested some helical display, as sketched in **Figure 4a**.

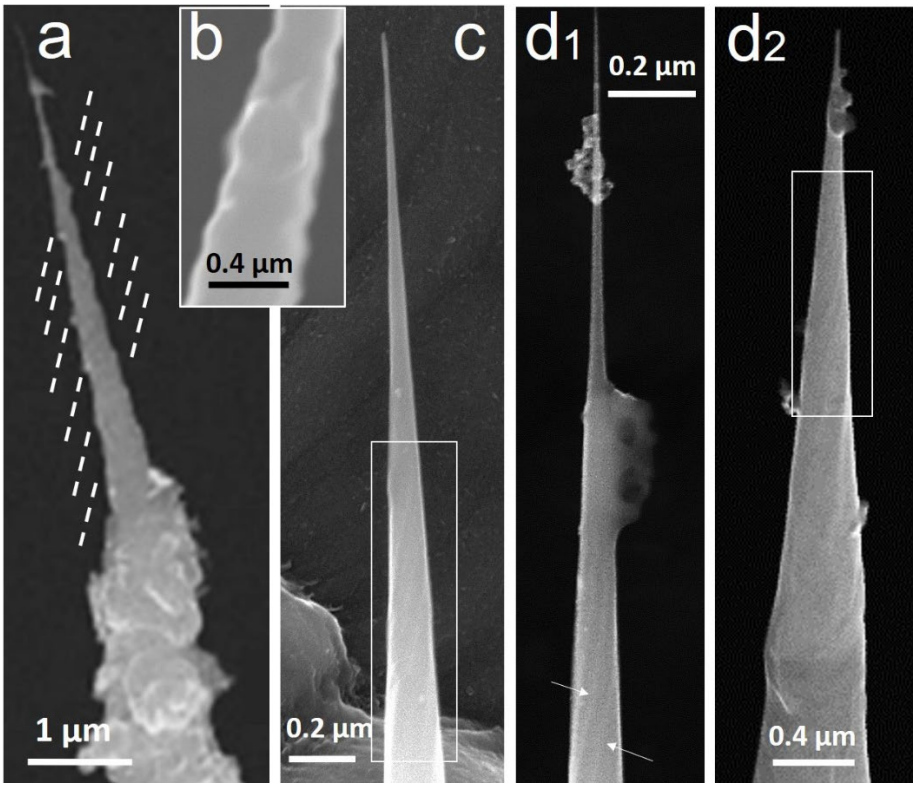

Figure 4. (a) to **(d)** SEM images of a variety of cones, all showing surface features suggesting a helical wrapping of the graphene layers making the cones, although the related contrasts are very faint (framed or arrowed areas in (c), (d_1), and (d_2)), except for the cones in (a) and (b) for which the wrapping is suggested by the positions of the opposed surface bumps. (d_1) and (d_2) are the same cone, before and after using it as a probe for Kelvin force microscopy (KFM) experiments. The fact that the helical features are visible in both images, yet faint, demonstrates that they are not some kind of image artefact.

A helical display on the cone surface is also suggested by faint lines, as arrowed in **Figure 4d$_1$** or in the framed areas of **Figures 4c** and **4d$_2$**. It is assumed, then, that those faint lines are the edges of graphene layers helically wrapped around the cone axis. The number of graphenes in each of the layers involved should be small, *e.g.*, 3-5, hence the steps formed by the layer edges are at the limit of the SEM resolution. This suggests also that other edges/steps may be present but cannot be seen because made of a lower number of graphenes, down to 1. Such a helical display of graphene layers at the carbon cone surface is not unprecedented. Other works having dealt with carbon cones prepared following different routes (*e.g.*, microwave plasma[15] or a combustion flame method[16]) showed obvious evidences of it. The spontaneous scroll-like wrapping of graphenes while being formed onto a Si substrate by chemical vapor deposition in a hydrogen–methane gas mixture activated by a direct current discharge was also demonstrated.[17] Correspondingly, the authors also found electron diffraction evidences of the similarity in the helicity vector for the graphene turns of a same scroll.[17]

The first helical wrapping of graphene layers to form a conical morphology was evidenced by Bacon in 1960[18] (**Figure 5**). Bacon[18] was looking for demonstrating how the graphenes were displayed in so-called "graphite whiskers" formed by an electric arc method (**Figure 5a**), at a time where the resolution power of SEM was not sufficient to directly image the surface steps formed by the graphene edges. the graphitic structure was demonstrated by electron diffraction, but the helical wrapping of the graphene layers could only be suspected. In order to ascertain it, a "large" current was passed through one of those whiskers, from which a crumpled graphene flake was obtained (**Figure 5b**), resulting from the unwrapping of the constituting graphene layers. Hence, the scroll-like model sketched as **Figure 5c** was proposed. Such a behavior was supported later on by calculations which demonstrated the spontaneous unwinding of a spirally-wrapped graphene upon charge injection.[19]

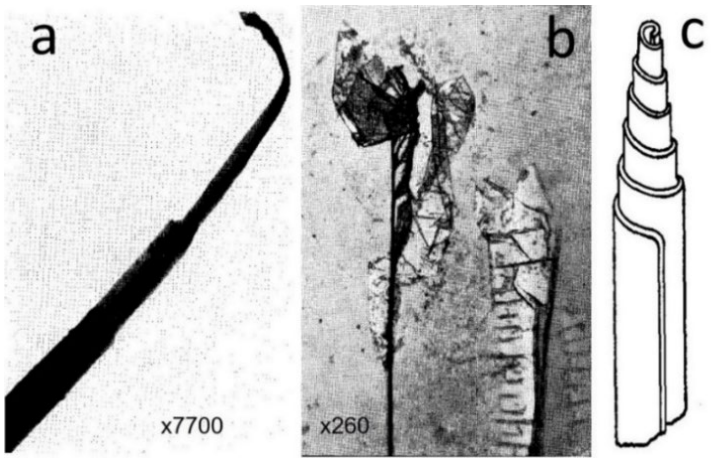

Figure 5. (a) TEM image of a graphite whiskers. **(b)** Optical image of an electrically exploded whisker. The current was said "large" in the paper, but the actual value was not provided (nor the voltage). **(c)** Textural model for a graphite whisker. All images reprinted with permission from Bacon, R. Growth, Structure, and Properties of Graphite Whiskers. *J. Appl. Phys.* **1960**, *31*, 283-290,[18] Copyright 1960 by AIP Publishing.

Because the SEM images of our cones were at the resolution limit, hence not enough to strongly support the hypothesis of a scroll-like model, an experiment similar to that of Bacon was attempted. An object similar to that of **Figure 1a** was welded with tungsten by a focused electron beam ion deposition process (FEBID)[7] onto an Au tip previously obtained by electrochemical etching and tapering (see Section 1 in **Supplementary Information**), resulting in the assembly shown in **Figure 6a**. Such Au tips are commonly used as probes for scanning tunneling microscopy (STM).

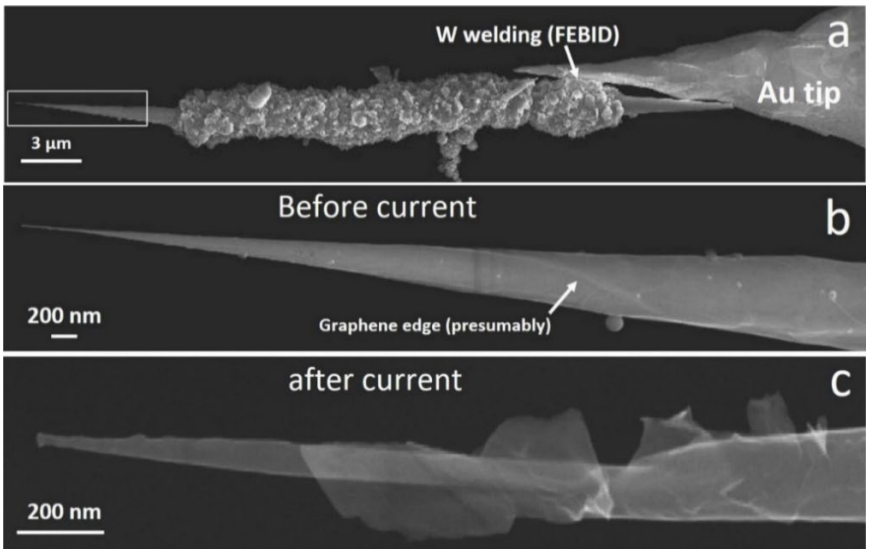

Figure 6. SEM images. **(a)** Overall view of a carbon-cone-bearing object welded onto an Au tip used as a STM probe. **(b)** Enlarged view of the area framed in (a). **(c)** The same carbon cone as in (b) after a current was passed through it.

Interestingly, the carbon cone surface was also showing a curved line-like contrast suggesting the presence of at least one graphene-edge step with sufficient thickness for being seen (**Figure 6b**, arrow). The carbon-cone-terminated Au-tip was then put within a STM, hence actually replacing the regular Au probe. Then a current was passed through it, first of 2 nA at 1.1 V, and then of 5 nA at 0.25 V. As a result, a similar unwrapping phenomenon as it was observed by Bacon (**Figure 5b**) was observed here (**Figure 6c**). Therefore, the concentrically display of the graphenes within the cones, which was previously ascertained by TEM[9] (**Figure 3**), combined with the evidences of wrapping (**Figure 4** + **Figure 6**) demonstrate that the texture of our cones is similar to that of Bacon whiskers sketched in **Figure 5c**, *i.e.*, it follows, at least partly, the scroll model, instead of the only Russian doll model initially proposed.[12] Why "partly" will be discussed in the next section. Anyway,

the scroll model is fully consistent with the fact that at least many of the concentric individual graphenes exhibit the same helicity vector.

Incidentally, it may be wondered, then, why the unwrapping phenomenon induced at the cone apex by subjecting the cone to some current or voltage has not prevented the carbon cones to make excellent electron emitters with high beam coherence. Indeed, cones were shown to be able to withstand emission currents as high as 30 μA and extraction voltage as high as ~1.3 kV[1-3] which is far beyond the range used here during the STM testing. The reason might be that all the cones mounted as electron emitters were welded by focused ion beam-induced deposition (FIBID) instead of FEBID, which was shown to be responsible for an extensive amorphization of the cone surface over an undetermined thickness, and of the cone apex.[7] Because of the amorphization, the graphene free-edges at the cone surface no longer exist and the related carbon atoms are welded to the bulk, hence hindering any unwrapping of the graphenes.

The possible occurrence of local coherent stacking in the cones. Thanks to the use of an 80 kV-operated TEM which prevents the atom planes from rapid irradiation damaging, aberration-corrected high-resolution images show that the graphenes constituting the cones are perfect (**Figure 7**).

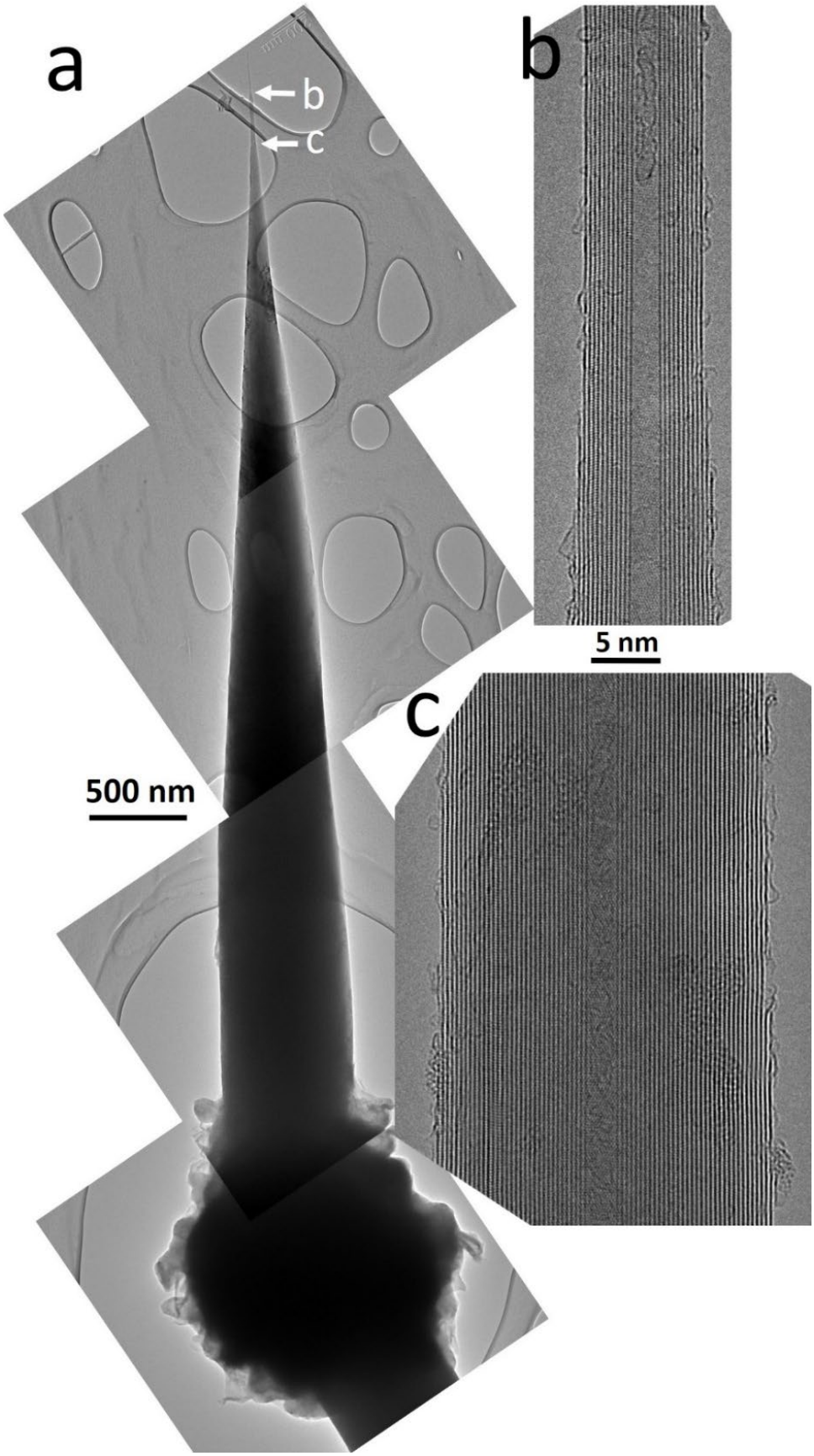

Figure 7. TEM images (80 kV). **(a)** Overall view of a carbon cone protruding from a small rough-surface carbon bead. **(b)** HRTEM image of the area arrowed "b" in (a). **(c)** HRTEM image of the area arrowed "c" in (a).

Figure 7b indicates that the part arrowed as "b" in **Figure 7a** contains the equivalent of about 10 concentric graphenes (actually turns of the scroll). The part arrowed as "c" contains the equivalent of 30-35 scroll turns (**Figure 7c**), *i.e.*, already three times more than in "b", despite both areas are close with respect to the whole length of the cone. Hence, the number of scroll turns increases rapidly with the cone diameter, and calculations provide an estimate of ~1000 scroll turns and/or concentric graphenes for a cone base ~670 nm large, as the one imaged in **Figure 7a**. **Figures 7b-c** also show that most of the graphene steps at the cone surface responsible for the conical morphology involve single graphenes. But graphene steps involving a higher number of graphenes were also found (**Figure S1** in **Supplementary Information**), consistently with the fact that some graphene steps are visible in SEM images (**Figures 4c-d** and **6b**).

The fact that concentric graphenes exhibit the same helicity vector allows the atoms of each of the layers to be in exact superimposition along the cone axis direction, hence to be in coherence. In principle, this is not the case when considering the atoms of each layers along the cone circumference, which induces an increasing shift between each graphene lattice with respect to the top layer along the circumference, and with the decreasing radius of curvature as well. However, the limited distortion induced to the graphene lattice by radii of curvature in the range of several hundred nanometers could allow coherent stacking situations to occur (i.e., not only AB-type, but also AA, AB', *etc.*) as soon as the concentric graphenes involved exhibit the same helicity vector. This is confirmed by a simple calculation (see Section 2 and **Figure S2** in **Supplementary information**): when considering a series of concentric graphenes spaced by 0.34 nm, of which the top one was applied a radius of curvature of 200 nm, a distance of 7.5 nm is required for the atoms from the lattices of the first two layers to be shifted by a maximum of 5% at their edges. Likewise, a number of piled-up layers up to 30 is required for the second atom of a pair of atoms to be shifted by 5% from the position of exact superimposition with respect to the equivalent pair of atoms from the first (top) layer. Therefore, considering a reference line parallel to the cone axis for which all the atoms of all the layers are perfectly superimposed as in AA stacking, and considering the increasing lattice shifts on both sides from this line, it is possible to get ribbon-like coherent domains (hence possibly several hundred nanometers long, actually the length of the outer cylinder or turn) up to a maximum width of 15 nm (if involving 2 layers) or less (if involving more layers) with a maximum atom shift of 5% at the domain edges with respect to the top layer. It is assumed that, for such a domain with slightly distorted lattice, the distortion is sufficiently low that the coherence is not significantly affected. As an example, using the calculation principles reported in Section 2 of **Supplementary Information**, and still applying a radius of curvature of 200 nm to the top layer, a 5-layer wedge-ribbon-like graphite domain for which the atom position shifts reach a maximum of

5% at the edge of the domain would have a width of ~3 nm (actually a 2.92 nm width for the top layer, and a 2.89 nm width for the bottom layer).

Considering the huge number of concentric individual graphenes involved in a cone, it is doubtful that a whole cone is built from a single graphene scrolled while forming a thousand turns. It is very likely that the cones are built from several, intricated scrolls. In addition, growth mechanisms determined in Paredes *et al.*[10] and reminded with **Figure 2** involve two concomitant ways for the cone to grow, one by the carbonization of a polyaromatic-hydrocarbon (PAH)-rich liquid migrating at the cone surface, the other by the accretion of carbon radicals to the graphene edges. It is reasonable to assume that the latter way generates a scroll where all the graphene turns necessarily exhibit the same helicity vector as it is a common way for crystals to grow when starting from a screw dislocation, while the former way is more likely to generate genuine concentric graphenes (*i.e.*, not scroll turns) with independent helicity vectors. Hence, both configuration (scroll, and Russian doll) may co-exist within the same cone, which is still consistent with the feature of the experimental electron diffraction patterns. Such a multi-scroll texture, also combined with concentric (cylindric) graphenes, was already hypothesized by Amelinckx *et al.*[20] to account for TEM features specific to arc-prepared MWCNTs. A tentative scenario to explain how such a complex texture for the carbon cone could possibly build up is provided in **Figure S3** and related comments in **Supplementary Information**.

Cone apex. The TEM study showed that the carbon cone apices are not all alike, because it depends on how each supporting CNT breaks so that individual carbon cone-bearing objects can be released. The breakage is not controlled and may be more or less stressing to the graphene lattice depending on the breakage conditions, to the extent that part of the lattice can be amorphized. Two examples of carbon cone apices are shown on **Figure 8**, among which **Figure 8b** shows such a local amorphization. **Figure 8b** also well illustrates the steps formed by the graphene edges present at the cone surface, confirming that most are single-layer graphenes, hence invisible by SEM. A close look at the cone apices shows how graphene terminations look like when graphene steps at the cone surface involve two superimposed graphenes instead of one, single graphene steps being more frequent on the main cone body (see **Figure 7b-c** and also **Figure S1**). The closer the graphenes to the apex, the higher the chance for having neighboring, superimposed graphene edges. Such a configuration and high temperatures (1400°C in our case) promote the closure of the graphene pairs with each other without inducing any additional curvature to the graphenes involved but in the closing part, as they look like they are merely zipped together (solid, red arrows in **Figures 8a-b**). This graphene termination is different from the termination which is modelled in **Figure 8** (black, dashed frame) and it is actually present on the apex of **Figure 8a** (black, dashed arrow). For this reason, in contradiction with the designation we formerly used,[21] we find more appropriate to

designate the double-graphene termination with the matchhead profile (black arrow) as "loop-like", and the double-graphene terminations with no deformation (red arrows) as "zip-like".

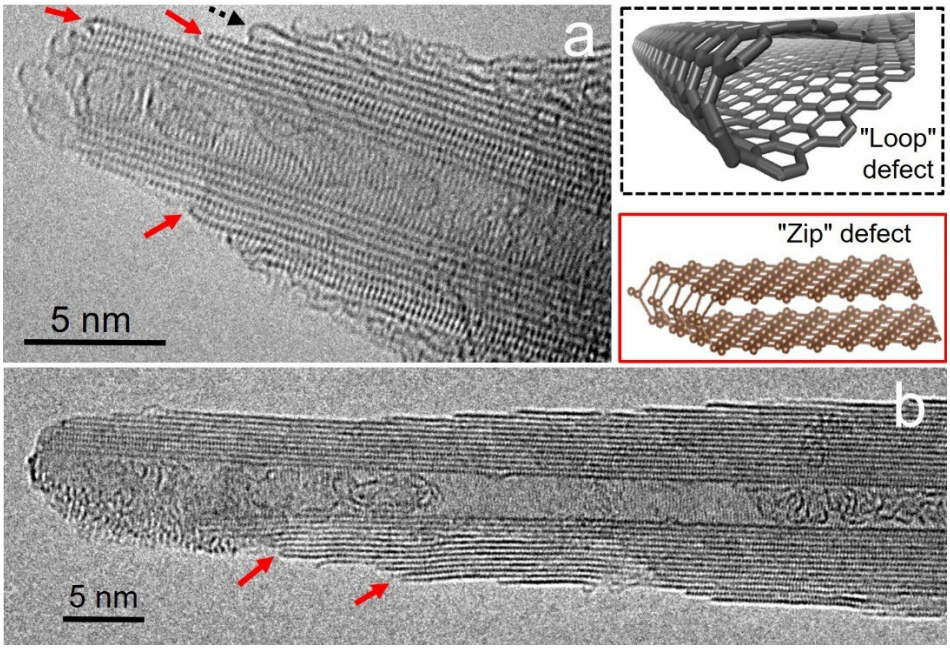

Figure 8. (a) and **(b)** TEM images (80 kV) of two cone apices. Red (solid) arrows designate zip-like terminations as coarsely sketched in the red frame aside. The black dashed arrow designates a loop-like termination as sketched in the black, dashed frame. The number of zip-like terminations is higher than imaged, because it is likely that only few are oriented properly with respect to the incoming electrons. Image in (a) is reprinted with permission under a CC-BY license from Puech *et al.* Analyzing the Raman Spectra of Graphenic Carbon Materials from Kerogens to Nanotubes: What Type of Information Can Be Extracted from Defect Bands? *'C'* **2019**, *5*, 69,[21] Copyright 2019 by the Authors.

It is worth noting that lip-lip interactions between superimposed graphenes which close on each other is a common observation for graphene-based objects grown or annealed at high temperatures, such as polyhedral crystals,[16,22] platelet nanofibers,[23] whiskers,[24] graphene nanoribbons,[25] pyramidal hillocks,[26] among others. But the resulting graphene terminations usually adopt the loop-like profile as sketched in **Figure 8** (black frame) so that to enable the graphene to curve and close while minimizing the strain on bond angles (see Section 3.1 and **Figure S4** in **Supplementary Information**). But such a configuration is not the preferred one here, and superimposed graphene lips close on each other into zip-like terminations without inducing curvatures to the graphene involved, or at minima. The zipping mechanism occurs when superimposed graphenes have their edges close to each other, as the carbon atoms from both graphenes try to bond to each other, possibly helped by the accretion of extra carbon atoms from the gas phase, in order to lower the system energy by eliminating the dangling bonds. The event is certainly facilitated by the fact that the graphene layers exhibit the same helicity, as previously demonstrated. This suggests that the atomic structure of the zip termination is different from that of a loop, and instead of being a bent

defect-free single-graphene lattice involving sp^2-C atoms only, it has to be another structural configuration possibly involving heterocycles, or a line of sp^2-C atoms with a partial sp^3 character, because of the need to connect the lips of two concentric graphene lattices whose the innermost one offers less carbon atoms to bonding than the outermost one. Such a configuration is not unique to our cones, though, as it can also be guessed in refs.[22,27] although images are less clear than in **Figure 8a-b**.

In order to determine whether zip-like terminations are structurally possible and stable, which kind of display and hybridization the carbon atoms could adopt to form them, and whether such a termination could actually form in our furnace conditions, atomistic modelling was carried-out (see the Methods section at the end). The starting configuration of the model was a system combining four concentric single-layer graphenes (*i.e.*, similar to single-wall carbon nanotubes) with an intergraphene distance of 0.355 nm, all of the zig-zag type. The two innermost tubes (of 2.97 and 3.68 nm diameters, respectively) percolate through the periodic boundary along the z-axis, making them virtually infinite. The two outermost tubes (of 4.38 and 5.09 nm diameters, respectively) were given the same finite length, so that to mimic the configuration of concentric graphenes in a cone (**Figure 9**, left).

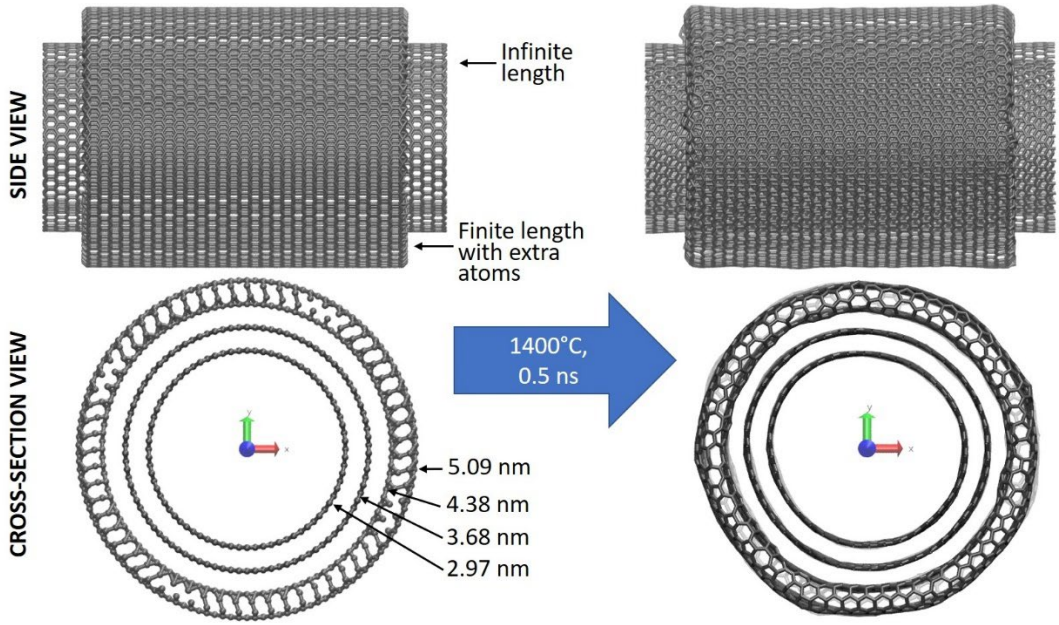

Figure 9. (Left) The four-concentric-nanotube system (zigzag configuration) built to model the situation at the nanocone surface when two graphene edges are at the same level. Additional carbon atoms are placed near the edges along two circles on both ends of the CNTs with finite length to facilitate edge reconstruction; top: side view; the carbon atom circles are too close to the graphene edges for being discriminated from them; bottom: cross-section view. **(Right)** the same system as on the left after 500 ps of molecular dynamics at 1400°C followed by 25 ps relaxation.

It was verified that the presence of the innermost CNTs with infinite length helped to better mimic the cone configuration (see Section 3.2 and **Figures S5-S6** in **Supplementary Information**). The zipping event, if any, certainly occurs at the very final step of the growth process, as it prevents the graphenes involved to grow further. Therefore, extra carbon atoms were then provided to the system along circles of arbitrary diameters of 4.62 and 4.93 nm, respectively, and located at 0.05 nm (along the nanotube axis) from the free edges of both ends of the two outermost CNTs. The goal was to mimic the ultimate input of carbon atoms which may occur at the very end of the growth step, once the $CH_4 + H_2$ gaseous supply is turned off and replaced by an argon flow.

After running the molecular dynamics simulation at 1400°C for 500 ps, then relaxing the system at room temperature for 25 ps, the spontaneous closure of the two outermost graphene edges on each other occurred (**Figure 9**, right). Such a closure was not ascertained because it could have been hindered by the cylindric curvature and the mismatch between the lattices of the two finite outermost tubes, which do not contain the same number of atoms due to their difference in diameters. A closer look to the atomic structure of the termination after heating and relaxation shows that the closure was made possible by the formation of many heterocycles (*i.e.*, aromatic rings made of a number of carbon atoms other than 6) (**Figure 10**, left).

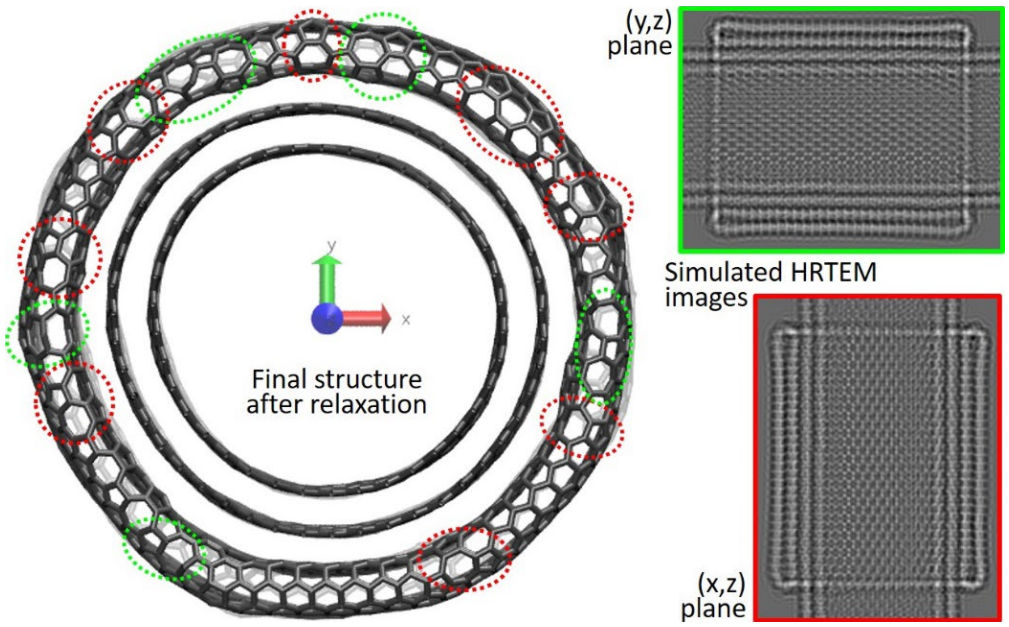

Figure 10. Left: enlarged view of the four-CNT system cross-section after heating and relaxation already shown on the bottom right of **Figure 9**. In order to help locating the occurrence of heterocycles in the distorted lattice of the zipped graphene termination, areas visibly containing some of them are circled. Red dashed circles show examples of the occurrence of 5- and 7-atom rings. Green dashed circles show the same but also involving 8-atom rings. **Right:** Calculated HRTEM images (C_s = 1 µ, defocus = 5 nm) of the side view of the system projected in the *yz* plane (green-framed image on top) and in the *xz* plane (red-framed image on bottom).

It is worth noting that, although closing the graphene lips with hexagonal rings only would not be possible because of the mismatch between both lattices, the number of heterocycles seen in the simulated image of **Figure 10** could be overestimated because of the (short) simulation timescale. Some of them could possibly rearrange to hexagons if the simulation was run for longer time. Calculated projected HRTEM images of the relaxed system according two directions *x* and *y* (**Figure 10**, right) shows that, interestingly, the termination does not adopt the loop-shape sketched in **Figure 8** (black, dashed frame), but the graphene lattices remain more or less parallel instead. The resulting calculated images of the terminations (**Figure 10**, right) mimic well the graphene terminations arrowed in red in the experimental HRTEM images (**Figure 8**).

It was confirmed that the behavior of the system is similar if the concentric nanotubes are all given the armchair configuration (**Figure S7** in **Supplementary Information**).

Both graphene terminations as modelled in **Figure 8** top right (loop) and **Figure 10** (zip) will be seen as defects by Raman spectroscopy. Raman spectra of carbon materials are composed of different Raman emission bands (G, D, D' and 2D bands, characterized by their intensity, width, and wavenumber[28]) which provide an accurate characterization of the graphenic carbon structure and nanotexture: *(i)* the D band (around 1330 cm^{-1}) results from a double resonance process and originates from the inelastic scattering of an electron by a defect (*e.g.*, graphene edge, vacancy, 5-7 ring pairs…) or more generally by a modification of the periodicity; *(ii)* the G band (around 1580 cm^{-1}) represents the collective vibration of in-plane C-C bonds in graphene; *(iii)* the D' band (~1620 cm^{-1}) is not much studied, but it also relates to defects as the D band, and by using both the D and D' bands, it is possible to discriminate the type of defects;[29] *(iv)* the 2D band (~2700 cm^{-1}) is both related to the number of graphenes and stacking type. All these bands are present in the Raman spectrum of a carbon cone apex (**Figure 11**), which was able to be obtained thanks to the accurate piezo-driven displacement of the Raman probe stage.

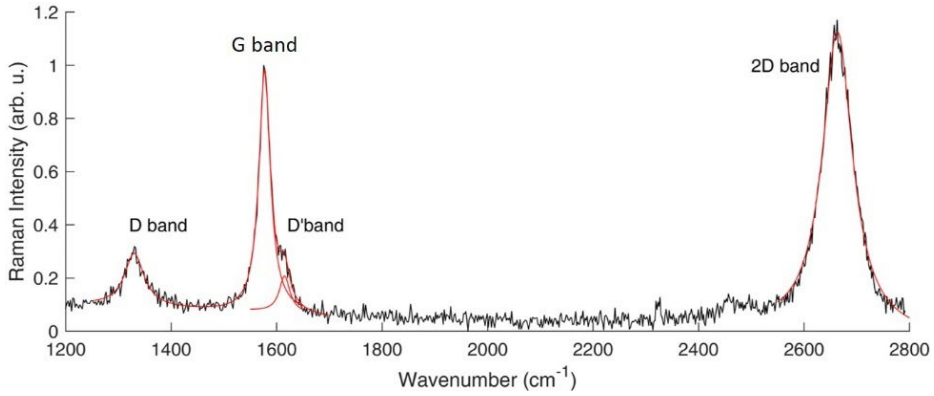

Figure 11. Raman spectrum recorded from the apex of a carbon cone. Black line is the experimental spectrum; red lines are the fits.

Beside the I_D/I_G intensity ratios, obtained on various places along the cone up to the rough-surface fiber-segment part, which are reported elsewhere,[21] we considered the work by Eckmann *et al.*,[29] who designed single-layer graphenes so that they contain a single type of defect, while varying the defect type. Eckmann *et al.* were able to assign $I_D/I_{D'}$ ratio values of 13, 7, and 3.5 as specific signatures of the presence of sp^3-C atoms, vacancies, and domain boundaries, respectively. Calculating the $I_D/I_{D'}$ ratio obtained from **Figure 11** on the cone apex, a very low value of ~1.5 was obtained, whereas $I_D/I_{D'}$ values were higher anywhere else on the cone.[21] Therefore, it does not correspond to any of the defects already identified in the literature. Because the cone apex is where the so-called "zip" defects were specifically found (as opposed to anywhere else in the cones), it is assumed that $I_D/I_{D'}$ ~1.5 could be their specific Raman signature. Although the zip-like terminations do not look many in **Figure 8**, they are surface defects, hence their signal is emphasized with respect to that from the rest of the material because of the low penetration depth of the Raman probe in graphenic materials (~90% of the Raman emission come from the first few tens of nanometers, considering a penetration depth $d = \lambda/(4\ \pi.\kappa)$, where the extinction coefficient κ *is* ~1.35 for λ = 632.8 nm[30]). It may also be wondered whether Eckmann's results, which were obtained on 1LG, may actually be compared to ours, which are involving a minimum of two layers contributing to zip-like termination, and more layers if we considered the graphenes underneath, hence more alike few-layer graphene (FLG). In case of FLG with incoherent stacking (which is definitely the case at the cone apex, where radii of curvature are small), the inter-layer interaction is weak, hence it does not change the shape of the Dirac cone, except at very low electron-hole energy. Consequently, as the D and D' bands are associated to electrons and holes with a large energy (half the excitation energy), it is reasonable to assume a similar Raman response between 1LG and incoherent FLG.

Our cones are not the only carbon materials the Raman spectra of which exhibit D and D' band intensities allowing ratio values in the same range to be anticipated. It is the case in some amorphous diamond-like carbon materials (DLC) heat-treated up to 2800°C.[31] This confirms that our very low $I_D/I_{D'}$ values are not due to some experimental artefact. It also suggests that, in the course of the extensive graphenization which is promoted in the DLC material by such high temperature treatments, zip-like terminations are formed.

The reason why $I_D/I_{D'}$ reaches such a low value because of the specific zip defect may relate to charge effects. Calculations showed that even moderate buckling of a graphenic structure may induce a flexoelectric behavior able to generate dipole-dipole interactions at the nanoscale.[32] From the point of view of Raman emission, it was calculated that polarizing a graphene structure may lower significantly the D band intensity, without affecting the D' band.[33] Therefore, the extreme deformation enforced to the bond angles of the carbon atoms joining the two graphene edges could result in such a strong polarization by concentrating charges at the zip-like termination, which is

helped by the lower carrier mobility at this very location because of the presence of many heterocycles (**Figure 10**), hence the very low $I_D/I_{D'}$ ratio value.

It is now interesting to compare the $I_D/I_{D'}$ ratio for the zip defect to that of the "loop" defect, an example of which was shown in the cone apex of **Figure 8a** (see the black dashed arrow in the experimental image, and the related sketch aside). A value of ~9 was recently obtained by Picheau *et al.,*[34] as a result from the Raman study of flattened CNTs obtained from the spontaneous collapsing of large diameter, few-wall CNTs. By combining our results with those from Eckmann *et al.*[29] and that from Picheau *et al.*,[34] the following identification chart can be proposed (**Table 1**):

Table 1. Identification chart of various defects able to affect the graphene lattice in graphenic carbons (revised and completed from ref.[21]).

Type of defects	$I_D/I_{D'}$	Ref.
sp^3-C	13	29
Loop	~9	34
Vacancy	7	29
Boundary	3.5	29
Zip	1.5	This work

Of course, it is likely that most of carbon materials contain more than one type of defects on a regular basis, hence resulting in $I_D/I_{D'}$ values being a mixture of some of the signature values reported in **Table 1**. But such a chart could help reveal trends, in relation with the synthesis conditions for instance.

CONCLUSION

High temperature (1400°C) time-of-flight CVD of pyrolytic carbon onto individual CNTs as supports is able to generate graphenic carbon cones made of concentric graphenes with perfect nanotexture. The work demonstrates that the concentric graphenes are actually turns of a scroll-like instead of Russian-doll-like texture. This shows the evidence of a scroll-based growth mechanism in CNT-related textures, otherwise only hypothesized in the literature so far, for instance based on merely observing a mismatch in the number of fringes on both sides of a CNT axis. Therefore, carbon cones prepared following the ToF-CVD route definitely grow according to the scroll model instead of the Russian-doll model. However, it is unlikely that a single cone corresponds to a single

scroll. The same cone might contain several intricated scrolls, possibly combined with a minor occurrence of the Russian-doll texture as suggested by the evidence for the co-existence of two different species responsible for the growth, *i.e.* polyaromatic hydrocarbons (PAHs) in liquid phase on the one hand, and small radicals on the other hand.[10] As allowed by the presence of concentric graphenes sharing the same helicity vector combined with the limited lattice shifts induced in curved graphenes for very long radii of curvature (several hundred nanometers), the conditions for the occurrence of coherent stacking may be locally reached in the cones, in spite of the curved nature of the graphenes involved. Molecular dynamics modelling showed that, at least in the synthesis conditions used, zipping two neighboring concentric-graphene edges to each other is possible and fast, thanks to the formation of many aromatic rings other than the regular 6-atom rings (*i.e.*, typically, rings made of 5, 7, and 8 carbon atoms). The resulting severely-curved zip-like graphene terminations are stable at room temperature, and actually found at the cone apex. It is proposed that this particular highly-curved, heterocycle-rich graphene termination exhibits a specific Raman signature, identified by a very low $I_D/I_{D'}$ ratio of 1.5. The work strengthens the relationship previously made by Eckmann *et al.*[29] between the Raman $I_D/I_{D'}$ band ratio and the type of defect present in the material, and completes it by proposing a chart for the identification of defects in graphenic materials.

METHODS

Experimental. Carbon cones were obtained using a CVD furnace starting from a feedstock of CH_4 and H_2. Individual CNTs were grown first at 1100°C using regular conditions involving iron nanoparticles as a catalyst, and then, in a second step, pyrolytic carbon was deposited on them for about 2 hours, forming all-graphene morphologies such as illustrated in **Figure 1**. In order to obtain them, three main conditions are needed: *(i)* the CH_4/H_2 ratio should be appropriate, and different from that used for growing the CNTs by decreasing the proportion of H_2; *(ii)* the temperature should be risen up to 1400°C; *(iii)* a furnace with a long isothermal zone should be used, in order to allow the appropriate species to form within the gas phase and then to condense as a transient liquid onto the CNTs. Therefore, the time of flight (in the time range of 1 minute) of the species within the gas phase is a key parameter, hence the "ToF-CVD" denomination. Further information about the synthesis conditions can be found in Allouche *et al.*.[9]

Cones were investigated by a Zeiss LEO 1540XB SEM equipped with a Gemini column and a Schottky-type electron source, and operated at 20 kV, providing a point resolution of ~1.1 nm.

Cones were also investigated by a FEI (Thermo Fisher Scientific) Titan Cube HRTEM equipped with a Schottky-type electron source and a C_s-corrector for the objective lens, operated at 80 kV, providing atomic resolution.

Modelling. A simplistic model of the nanocones was created to investigate the ability of free graphene-edges to close and the structure of the reconstructed graphene termination. The atomistic modelling of the way the edges of two concentric graphenes behave at 1400°C in presence of extra carbon atoms was carried out using an in-house molecular dynamics (MD) code, operating in the canonical ensemble at a fixed temperature of 1400 °C, *i.e.*, identical to that of the growth step. Interactions between carbon atoms are described with the AIREBO potential[35] as modified in Farbos *et al.*.[36] It comprises the adaptive introduction of the Lennard-Jones potential specific to AIREBO, but the useless single bond torsional term is removed and the bond order parameters are set back to the original second generation REBO potential.[37] Equations of motions are integrated with a velocity Verlet algorithm[38] using a 0.2 fs timestep. Temperature is fixed with the stochastic thermostat of Andersen[39] with a high collision frequency $\tau = 5x10^{14}$ s^{-1} at 1400°C, to quickly dissipate the heat produced by the edge reconstruction in the early stages of the simulation. Room temperature relaxation is performed with a much milder thermostat setup: $\tau = 1x10^{13}$ s^{-1}. Related HRTEM images were simulated from the different models using the multislice simulation package *Dr Probe*.[40] A voltage of 80 kV, C_s = 1 µm, and defocus = 5 nm were considered in the simulation conditions for comparison with the experimental images.

Finally, cones were investigated by Raman spectroscopy with an excitation wavelength of 632.8 nm using a laser spot size of 0.5 µm and a power of 0.7 mW. Spectra were recorded for 200 s. The Raman spectrometer was coupled with a piezo-driven specimen stage. This allowed positioning accurately the laser probe onto single microsized objects as shown in **Figure 1a**, which was necessary to obtain spectra from the various parts of the object.

Throughout the paper, the terms "texture", "nanotexture", and "structure" are used according to the definitions provided in Monthioux *et al.*.[41]

ASSOCIATED CONTENT

Supporting Information is available free of charge at xxxxxxxxxxxxx

(i) Procedure for tapering Au wires; *(ii)* Additional HRTEM image; (*iii*) Details of the calculation for the possible dimensions of a coherent domain enabled by large radii of curvature of concentric graphenes; *(iv)* Tentative growth scenario for the cone parts; (*v*) Further data on modelling.

AUTHOR INFORMATION

Corresponding Authors

Germercy Paredes - *Laboratorio de Nanociencia, Pontificia Universidad Católica Madre y Maestra, Santiago de Los Caballeros 51000, Dominican Republic*; orcid.org/ 0000-0003-4983-0948; Email: gd.paredes@ce.pucmm.edu.do

Marc Monthioux - *Centre d'Elaboration des Matériaux et d'Etudes Structurales (CEMES), UPR8011 CNRS, Université Toulouse 3, 31055, Toulouse, France*; orcid.org/0000-0002-7989-9746; Email: marc.monthioux@cemes.fr

Author Contributions

All authors have given approval to the final version of the manuscript. G.P. and M.M. have written the initial version of the manuscript. All authors have discussed the data and contributed to the subsequent versions until the final version. G.P. carried out the synthesis and part of the SEM investigation. R.W. and R.A. carried-out the HRTEM investigation. P.P. carried-out the Raman spectroscopy investigation. G.S. carried-out the STM experiment. J.-M.L. carried out the Molecular dynamics modelling. The original idea comes from G.P. and M.M. A.M., F.P., and M.M. have supervised parts of the work.

Notes

The authors declare no competing financial interest.

ACKNOWLEDGMENTS

This study has been supported through the EUR grant NanoX n° ANR-17-EURE-0009 in the framework of the "Programme des Investissements d'Avenir", the CNRS-funded International Research Project NEWCA, the Government of Aragon (project DGA E13-20R), the Spanish MICINN (PID2019-104739GB-100/AEI/10.13039/501100011033), the European Union H2020 programs "ESTEEM3" (Grant number 823717), and the "Graphene Flagship" CORE 3 (Grant number 881603). The Pontificia Universidad Católica Madre y Maestra (Santiago, Dominican Republic) is also thanked for providing the PhD grant for G. Paredes. R. Cours (CEMES) is thanked for carrying out the FEBID-assisted nano-welding of the carbon cones on the Au tip. M. Kandara and A. C. Torres-Dias are thanked for performing some of the SEM images. The HRTEM studies were conducted at the Laboratorio de Microscopias Avanzadas (LMA), Universidad de Zaragoza, Spain.

REFERENCES

(1) Houdellier, F.; Masseboeuf, A.; Monthioux, M.; Hÿtch, M. J. New Carbon Cone Nanotip for Use in a Highly Coherent Cold Field Emission Electron Microscope. *Carbon* **2012**, *50*, 2037-2044

(2) Houdellier, F.; de Knoop, L.; Gatel, C.; Masseboeuf, A.; Mamishin, S.; Taniguchi, Y.; Delmas, M.; Monthioux, M.; Hÿtch, M. J.; Snoeck, E. Development of TEM and SEM High Brightness Electron Guns Using Cold Field Emission from a Carbon Nanotip. *Ultramicrosc.* **2015**, *151*,107-115.

(3) Mamishin, S.; Kubo, Y.; Cours, R.; Monthioux, M.; Houdellier, F. 200 kV Cold Field Emission Source Using Carbon Cone Nanotip: Application to Scanning Transmission Electron Microscopy. *Ultramicrosc.* **2017**, *182*, 303-307.

(4) Kleshch, V. I.; Purcell, S. T.; Obraztsov, N. Single Crystal Diamond Needle As Point Electron Source. *Sci. Rep.* **2016**, *6*, 35260.

(5) Ota, K.; Kato, Y.; Teii, K. Formation of Nanocrystalline Diamond Cones by Reactive Ion Etching in Microwave Plasma for Enhancing Field Emission. *Jap. J. Appl. Phys.* **2019**, *58*, 016003.

(6) Shibata, T.; Unno, K.; Makino, E.; Shimada, S. Fabrication and Characterization of Diamond AFM Probe Integrated with PZT Thin Film Sensor and Actuator. *Sens. Actuat. A* **2004**, *114*, 398-405.

(7) Paredes, G. *Development of new probes based on carbon nanocones for near-field microscopies*. PhD Dissertation, University of Toulouse (France), **2020**.

(8) Jacobsen, R. L.; Monthioux, M. Carbon Beads with Protruding Cones. *Nature* **1997**, *385*, 211-212.

(9) Allouche, H.; Monthioux, M.; Jacobsen, R. Chemical Vapor Deposition of Pyrolytic Carbon on Carbon Nanotubes: (I) Synthesis and Morphology. *Carbon* **2003**, *41*, 2897-2912.

(10) Paredes, G.; Ondarçuhu, T.; Monthioux, M.; Piazza F. Unveiling the Existence and Role of a Liquid Phase in a High Temperature (1400 °C) Pyrolytic Carbon Deposition Process. *Carbon Trends* **2021**, *5*, 10017**.**

(11) Dong, G. L.; Hüttinger, K. J. Consideration of Reaction Mechanisms Leading to Pyrolytic Carbon of Different Textures. *Carbon* **2002**, *40*, 2515-2528.

(12) Allouche, H.; Monthioux, M. Chemical Vapor Deposition of Pyrolytic Carbon on Carbon Nanotubes. Part 2. Texture and Structure. *Carbon* **2005**, *43*, 1265-1278.

(13) Monthioux, M. Structure, Texture, and Thermal Behaviour of Polyaromatic Solids. In *Carbon Molecules and Materials*; Setton, R., Bernier, P., Lefrant, S., Eds.; Taylor & Francis, London (UK), **2002**; pp.127-177.

(14) Oberlin, A.; Goma, J.; Rouzaud, J.-N. Techniques d'Etude des Structures et Textures (Microtextures) des Matériaux Carbonés. *J. Chim. Phys.* **1984**, *81*, 701-710.

(15) Zhang, G.; Jiang, X.; Wang, E. Tubular Graphite Cones. *Science* **2003**, *300*, 472-474.

(16) Okuno, H.; Palnichenko, A.; Desprès, J.-F.; Issi, J.-P.; Charlier, J.-C. Synthesis of Graphite Polyhedral Crystals Using a Combustion Flame Method. *Carbon* **2005**, *43*, 692-697.

(17) Chuvilin, A. L.; Kuznetsov, V. L.; Obraztsov, A. N. Chiral Carbon Nanoscrolls with a Polygonal Cross-Section. *Carbon* 2009, **47**, 3099-3105.

(18) Bacon, R. Growth, Structure, and Properties of Graphite Whiskers. *J. Appl. Phys.* **1960**, *31*, 283-290.

(19) Braga, S. F.; Coluci, V. R.; Legoas, S. B.; Giro, R.; Galvão, D. S.; Baughman R. H. Structure and Dynamics of Carbon Nanoscrolls. *Nano Lett.* **2004**, *4*, 881-884.

(20) Amelinckx, S.; Bernaerts, D.; Zhang, X. B.; Van Tendeloo, G.; Van Landuyt, J. A Structure Model and Growth Mechanism for Multishell Carbon Nanotubes. *Science* **1995**, *267*, 1334-1338.

(21) Puech, P.; Kandara, M.; Paredes, G.; Moulin, L.; Weiss-Hortola, E.; Kundu, A.; Ratel-Ramond, N.; Plewa, J.-M.; Pellenq, R.; Monthioux, M. Analysing the Raman Spectra of Graphenic Carbon Materials from Kerogens to Nanotubes: What Type of Information Can Be Extracted from Defect Bands. *'C'* **2019**, *5*, 69.

(22) Gogotsi, Y.; Libera, J. A.; Kalashnikov, N.; Yoshimura, M. Graphite Polyhedral Crystals. *Science* **2000**, *290*, 317-320.

(23) Yoon, S.-H.; Lim, S.; Hong, S.-H.; Qiao, W.; Whitehurst, D. D.; Mochida, I.; An, B.; Yokogawa, K. A Conceptual Model for the Structure of Catalytically Grown Carbon Nano-Fibers. *Carbon* **2005**, *43*, 1828-1838.

(24) Saito, Y.; Arima, T. Features of Vapor-Grown Cone-Shaped Graphitic Whiskers Deposited in the Cavities of Wood Cells. *Carbon* **2007**, *45*, 248–255.

(25) Campos-Delgado, J.; Kim, Y. A.; Hayashi, T.; Morelos-Gómez, A.; Hofmann, M.; Muramatsu H.; Endo, M.; Terrones, H.; Shull, R. D.; Dresselhaus, M. S.; Terrones, M. Thermal Stability Studies of CVD-Grown Graphene Nanoribbons: Defect Annealing and Loop Formation. *Chem. Phys. Lett.* **2009**, *469*, 177–182.

(26) Glad, X.; de Poucques, L.; Jaszczak, J. A.; Belmahi, M.; Ghanbaja, J.; Bougdira, J. Plasma Synthesis of Hexagonal-Pyramidal Graphite Hillocks. *Carbon* **2014**, *76*, 330-340.

(27) Gogotsi, Y.; Dimovski, S., Libera, J. A. Conical Crystals of Graphite. *Carbon* **2002**, *40*, 2263-2284.

(28) Ferrari, A. C.; Basko, D. M. Raman Spectroscopy as a Versatile Tool for Studying the Properties of Graphene. *Nature Nanotechnol.* **2013**, *8*, 235-246.

(29) Eckmann, A.; Felten, A.; Mishchenko, A.; Britnell, L.; Krupke, R.; Novoselov, K. S.; Casiraghi, C. Probing the Nature of Defects in Graphene by Raman Spectroscopy. *Nano Lett.* **2012**, *12*, 3925–3930.

(30) Weber, J. W.; Calado, V. E.; van de Sanden, M. C. M. Optical Constants of Graphene Measured by Spectroscopic Ellipsometry. *Appl. Phys. Lett.* **2010**, *97*, 091904.

(31) Ribeiro-Soares, J.; Oliveros, M. E.; Garin, C.; David, M. V.; Martins, L. G. P.; Almeida, C. A.; Martins-Ferreira, E. H.; Takai, K.; Enoki, E.; Magalhaes-Paniago, R.; Malachias, A.; Jorio, A.; Archanjo, B. S.; Achete, C. A.; Cançado, L. G. Structural Analysis of Polycrystalline Graphene Systems by Raman Spectroscopy. *Carbon* **2015**, *95*, 646-652.

(32) Kothari, M.; Cha, M.-H.; Kim, K.-S. Critical Curvature Localization in Graphene. I. Quantum-Flexoelectricity Effect. *Proc. R. Soc. A* **2018**, *474*, 20180054.

(33) Venezuela, P.; Lazzeri, M.; Mauri, F. Theory of Double-Resonant Raman Spectra in Graphene: Intensity and Line Shape of Defect-Induced and Two-Phonon Bands. *Phys. Rev. B* **2011**, *84*, 035433.

(34) Picheau, E.; Impellizzeri, A.; Rybkovskiy, D.; Bayle, M.; Mevellec, J.-Y.; Hof, F.; Saadaoui, H.; Noé, L.; Torres Dias, A. C.; Duvail, J.-L.; Monthioux, M.; Humbert, B.; Puech, P., Ewels, C. P.; Pénicaud, A. Intense Raman D Band without Disorder in Flattened Carbon Nanotubes. *ACS nano* **2021**, *15*, 596-603.

(35) Stuart, S. J.; Tutein, A. B.; Harrison, J. A. A Reactive Potential for Hydrocarbons with Intermolecular Interactions. *J. Chem. Phys.* **2000**, *112*, 6472–6486.

(36) Farbos, B.; Weisbecker, P.; Fischer, H. E.; Da Costa, J. P.; Lalanne, M.; Chollon, G.; Germain, C.; Vignoles, G. L.; Leyssale, J.-M. Nanoscale Structure and Texture of Highly Anisotropic Pyrocarbons Revisited with Transmission Electron Microscopy, Image Processing, Neutron Diffraction and Atomistic Modelling. *Carbon* **2014**, *80*, 472–489.

(37) Brenner, D. W.; Shenderova, O. A.; Harrison, J. A.; Stuart, S. J.; Ni, B.; Sinnott, S. B. A Second-Generation Reactive Empirical Bond Order (REBO) Potential Energy Expression for Hydrocarbons. *J. Phys.: Condens. Matter* **2002**, *14*, 783–802.

(38) Allen, M. P.; Tildesley, D. J. *Computer simulation of liquids*, Oxford University Press, Oxford (UK) **1987**.

(39) Andersen, H. C. Molecular Dynamics Simulations at Constant Pressure and/or Temperature. *J. Chem. Phys.* **1980**, *72*, 2384.

(40) Barthel, J. Dr. Probe: A Software for High-Resolution STEM Image Simulation. *Ultramicrosc.* **2018**, *193*, 1-11.

(41) Monthioux, M.; Noé, L.; Kobylko, M.; Wang, Y.; Cazarès-Huerta M.; Pénicaud A. Determining the Structure of Graphene-Based Flakes from Their Morphotype. *Carbon* **2017**, *115*, 128-133.

FOR TABLE CONTENT ONLY